AGU PUBLICATIONS

JGR

Journal of Geophysical Research: Oceans

RESEARCH ARTICLE

10.1002/2015JC010872

Coupled dynamics of interfacial waves and bed forms in fluid muds over erodible seabeds in oscillatory flows

J. H. Trowbridge[1] and P. Traykovski[1]

[1]Department of Applied Ocean Physics and Engineering, Woods Hole Oceanographic Institution, Woods Hole, Massachusetts, USA

Key Points:
- Observations indicate interfacial waves on fluid muds in oscillatory flows
- Parametric instability does not explain the observed interfacial waves
- A mud-seabed system is unstable to bed forms and waves at the observed scales

Correspondence to:
J. H. Trowbridge,
jtrowbridge@whoi.edu

Citation:
Trowbridge, J. H., and P. Traykovski (2015), Coupled dynamics of interfacial waves and bed forms in fluid muds over erodible seabeds in oscillatory flows, *J. Geophys. Res. Oceans*, *120*, 5698–5709, doi:10.1002/2015JC010872.

Received 26 MAR 2015
Accepted 20 JUL 2015
Accepted article online 23 JUL 2015
Published online 16 AUG 2015

Abstract Recent field investigations of the damping of ocean surface waves over fluid muds have revealed waves on the interface between the thin layer of fluid mud and the overlying much thicker column of clear water, accompanied by bed forms on the erodible seabed beneath the fluid mud. The frequencies and wavelengths of the observed interfacial waves are qualitatively consistent with the linear dispersion relationship for long interfacial waves, but the forcing mechanism is not known. To understand the forcing, a linear model is proposed, based on the layer-averaged hydrostatic equations for the fluid mud, together with the Meyer-Peter-Mueller equation for the sediment transport within the underlying seabed, both subject to oscillatory forcing by the surface waves. If the underlying seabed is nonerodible and flat, the model indicates parametric instability to interfacial waves, but the threshold for instability is not met by the observations. If the underlying seabed is erodible, the model indicates that perturbations to the seabed elevation in the presence of the oscillatory forcing create interfacial waves, which in turn produce stresses within the fluid mud that force a net transport of sediment within the seabed toward the bed form crests, thus causing growth of both bed forms and interfacial waves. The frequencies, wavelengths, and growth rates are in qualitative agreement with the observations. A competition between mixing created by the interfacial waves and gravitational settling might control the thickness, density, and viscosity of the fluid muds during periods of strong forcing.

1. Introduction

1.1. Background

Measurements in a recent field investigation of the damping of ocean surface waves over fluid muds [*Traykovski et al.*, 2015] indicate waves on the density interface between the thin layer of fluid mud and the overlying much thicker column of clear water, accompanied by bed forms on the underlying erodible seabed, which contains significant quantities of noncohesive silt. Typical scales (Table 1) are a water depth of 7 m, a mud layer thickness of 0.1–0.3 m, a mud-water density contrast of 100–300 kg/m^3, and surface waves with a dominant period of 10 s, a dominant wavelength of 80 m, and velocities, just above the mud layer, of ten to tens of centimeters per second. Under these conditions, the observed interfacial waves (Figure 1) have the same dominant period as that of the surface waves, amplitudes of a few centimeters, and wavelengths of several meters, much shorter than the surface wavelength, and roughly consistent with the linear dispersion relationship for long frictionless interfacial waves over a flat fixed seabed, i.e.,

$$\omega^2 = g' h k^2 , \tag{1}$$

where ω and k are the dominant radian frequency and wave number of the interfacial waves, and g' and h are the reduced gravity and thickness of the mud layer. The interfacial waves respond rapidly to variability of the forcing by the surface waves, thus varying in amplitude on the time scale of the surface wave groups (Figure 1). The bed forms on the seabed beneath the fluid mud have amplitudes and wavelengths comparable to those of the interfacial waves, but they respond to the forcing on much longer time scales of hours to days. The interfacial waves are of interest because they have been hypothesized to influence the mixing that controls the thickness and density of the fluid mud [*Traykovski et al.*, 2015], which in turn determine the damping rate for surface waves [*Dalrymple and Liu*, 1978].

The relationship between the periods and wavelengths of the interfacial waves is roughly consistent with the long linear dispersion relationship (as noted above), but the mechanism by which these waves are forced is not known, and the mechanism that creates the bed forms and determines their scales is also not

Table 1. Observed [*Traykovski et al.*, 2015] and Model-Derived Characteristics of Fluid Mud Layers[a]

Quantity	Turbulent	Transitional	Laminar
ω = radian frequency of surface waves (s^{-1})	0.69	0.75	0.69
$\left(\overline{U_\infty^2}\right)^{1/2}$ = RMS undisturbed free-stream velocity (m/s)	0.51	0.23	0.09
h = undisturbed thickness of mud layer	0.10	0.31	0.22
ρ = density of fluid mud (kg/m^3)	1170	1280	1300
ν = kinematic viscosity of fluid mud (m^2/s)	9.0×10^{-4}	1.2×10^{-3}	4.2×10^{-3}
$\left(\overline{\eta^2}\right)^{1/2}$ = root-mean-square interfacial displacement (m)	0.056	0.052	0.008
$(\rho_\infty^2/\rho^2)\overline{U_\infty^2}/(g'h)$ = squared Froude number	1.57	0.05	0.01
$r/\omega=3\nu/(\omega h^2)$ = dimensionless damping rate	0.39	0.05	0.37
Wiberg and Harris [1994] anorbital ripple wavelength (m)	1.48	0.61	0.25
Minimum unstable wavelength from present model (m)	4.1	8.2	7.9
Fastest-growing wavelength from present model (m)	5.1	9.6	9.7
e-folding bed form growth time scale from present model (s)	7.7×10	1.3×10^5	2.3×10^4

[a]*Traykovski et al.* [2015] measured ω, $\left(\overline{U_\infty^2}\right)^{1/2}$, h, and $\left(\overline{\eta^2}\right)^{1/2}$ directly, and they estimated ρ and ν by fitting the vertical structure of the measured velocity profiles within the fluid mud to a model with constant density and viscosity, which is the vertically resolved analog of the present layer-averaged model for the undisturbed flow. The distinction between turbulent, transitional, and laminar cases is based on spectra of vertical velocity, which indicate a −5/3 power dependence on frequency, consistent with an inertial subrange, in the turbulent case, with suppression of the inertial range in the transitional and laminar cases. Computations from the present model are from the solution for the forced case with bed forms.

known. The observed bed forms are much longer than wave-formed orbital or anorbital sand ripples under similar forcing in clear water [e.g., *Wiberg and Harris*, 1994; *Traykovski*, 2007]. The observed interfacial wavelength is an order of magnitude larger than indicated by quasi-steady inviscid Kelvin-Helmholtz instability [e.g., *Drazin and Reid*, 2004]. The observed wavelength is an order of magnitude smaller and the observed amplitude an order of magnitude larger than indicated by a model [*Dalrymple and Liu*, 1978] in which surface waves over a mud layer of uniform density and viscosity force bound interfacial waves with the same frequency and wavelength as those of the surface waves. The observed frequency of the interfacial waves is twice that produced by a nonlinear mechanism [*Hill and Foda*, 1996, 1998, 1999; *Jamali et al.*, 2003a,2003b],

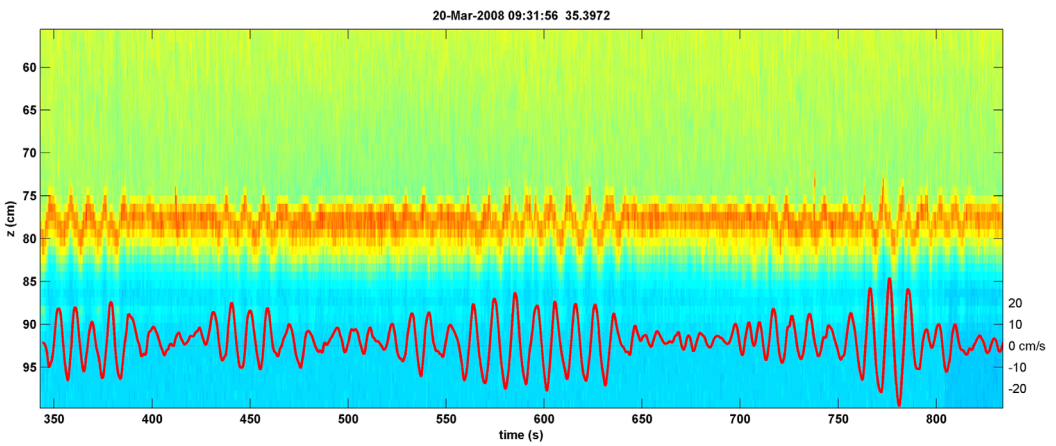

Figure 1. Acoustic backscatter imagery of interfacial waves at the top of a layer of fluid mud (color scale) and surface-wave-induced free-stream velocity above the mud layer (bottom red trace) from field measurements [*Traykovski et al.*, 2015] in the Gulf of Mexico off the Atchafalaya River outflow at a water depth of approximately 7 m. The acoustic imagery of the mud-water interface was obtained by a downward-looking pulse-coherent Doppler sonar with a frequency of 2.5 MHz, mounted 0.87 m above the seafloor. The color indicates echo intensity as a function of range, and the warm colors indicate the mud-water interface with wave-like oscillations. The surface-wave-induced velocity was measured by an acoustic Doppler velocimeter approximately 1 m above the seafloor. The scale on the left side of the figure is the downward distance from the sonar transducer, and the scale on the right side is the magnitude of the surface-wave-induced velocity. The mud layer thickness, determined by a hard echo from the seafloor based on accompanying 1.2 MHz acoustic imagery (not shown), was approximately 0.1 m. The record of wave-induced velocity indicates wave groups, a peak free-stream velocity of approximately 0.3 m/s, and a wave period of approximately 10 s. The acoustic imagery indicates waves on the mud-water interface with amplitudes up to approximately 0.04 m and a period equal to that of the surface waves. The wavelength of the interfacial waves is estimated at approximately 4 m based on a continuity argument and spatial measurements from a horizontal array. The density contrast between the fluid mud and the overlying clear water is estimated at approximately 200 kg/m^3. The interfacial waves occur during surface wave groups and disappear between wave groups.

in which standing interfacial waves at half the frequency of the progressive surface waves are generated by a triad interaction. The observed interfacial waves are not described by an analysis of Kelvin-Helmholtz instability in a viscous fluid mud subjected to steady forcing [*Harang et al*., 2014], as opposed to oscillatory forcing.

1.2. Present Study

Motivated by the observations, the present study is a linear analysis of the stability of the coupled system consisting of the fluid mud and the underlying erodible seabed in the presence of the oscillatory forcing by the surface waves. The objective is to identify a mechanism that can produce interfacial waves and bed forms with the observed frequencies, wavelengths, and time scales for growth.

The mathematical model (section 2) is based on the layer-averaged mass and hydrostatic momentum equations for the fluid mud, modeled as an incompressible Newtonian fluid with constant density and viscosity, and the conservation of mass equation and the Meyer-Peter-Mueller equation for the sediment transport in the underlying erodible seabed. The water depth and surface wavelength are assumed to be much longer than the thickness of the fluid mud layer and the wavelength of the interfacial waves and bed forms, so that the forcing by the surface waves can be represented by a spatially uniform temporally varying horizontal pressure gradient. The hydrostatic model of the fluid mud is consistent with the relatively small ratio of the observed interfacial and bed form wavelengths to the thickness of the mud layer. The incompressible Newtonian model, simpler than some previous rheological models of wave-seabed interaction, which have included not only Newtonian [e.g., *Gade*, 1958; *Dalrymple and Liu*, 1978; *Ng*, 2000; *Kaihatu et al*., 2007; *Wintertwerp et al*., 2007] but also viscoelastic [e.g., *Hsiao and Shemdin*, 1980; *MacPherson*, 1980; *Jiang and Mehta*, 1995] and viscoplastic [e.g., *Liu and Mei*, 1989], is adopted for simplicity and because of its success in interpreting recent field measurements [*Traykovski et al*., 2015]. The Meyer-Peter-Mueller equation for the sediment transport in the underlying erodible seabed is similarly adopted for simplicity and plausibility for sediments with significant silt fractions.

Three model solutions (section 3) for spatially periodic disturbances are presented. In the unforced case, the model indicates temporally damped modes, which cannot explain the observations. In the forced case without bed forms, the model indicates viscous parametric resonance of interfacial waves, closely related to the instability that creates surface waves in channel flow over a flat plate oscillating in its own plane [*Yih*, 1968; *Or*, 1997; *Gao and Lu*, 2006], but the instability threshold determined by the model is not met in the observations. In the forced case with bed forms, an approximate model solution indicates coupled growth of interfacial waves and bed forms, with frequencies, wavelengths, and time scales for growth that are qualitatively consistent with the observations.

A discussion (section 4) addresses the physics of the instability of the coupled mud-seabed system and the possible role of mixing created by the interfacial waves in controlling the thickness, density, and viscosity of the mud layer.

A summary and conclusions (section 5) is followed by appendices with mathematical details and a list of symbols.

2. Mathematical Model

2.1. Overview

The analysis addresses inviscid clear seawater of constant density ρ_∞ over fluid mud with constant undisturbed thickness h, density ρ, and viscosity ν, in turn over erodible sediment with porosity n and specific gravity s (Figure 2). The horizontal coordinate is x, time is t, and the gravitational acceleration is g. The spatially uniform horizontal pressure gradient produced by the surface waves is $\partial P/\partial x = -\rho_\infty dU_\infty/dt$, where $U_\infty(t)$ is the undisturbed velocity in the overlying clear seawater. The undisturbed overlying velocity is Gaussian and narrow banded, so that $\ddot{U}_\infty = d^2U_\infty/dt^2 = -\omega^2 U_\infty$, where dots indicate time derivatives and ω is the dominant radian frequency of the surface waves.

2.2. Mass, Momentum, and Sediment Transport Equations

The flow within the fluid mud is modeled by the layer-integrated mass-conservation equation:

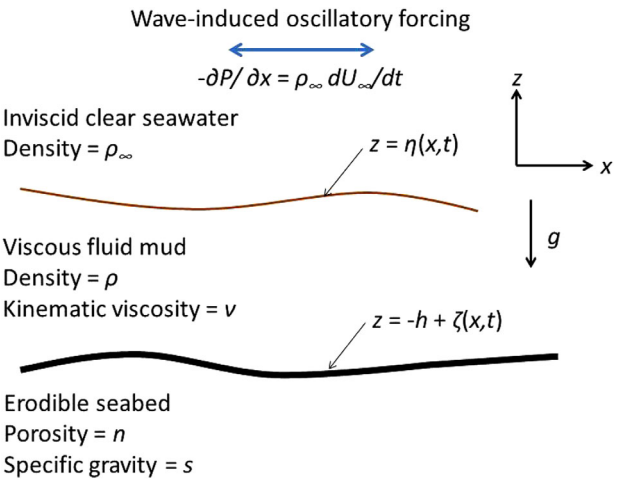

Figure 2. Diagram of the configuration addressed by the analysis. Inviscid clear seawater of density ρ_∞ overlies fluid mud of thickness h, density ρ, and viscosity ν, which in turn overlies an erodible seabed of sediment porosity n and specific gravity s. The system is forced by an undisturbed free-stream pressure gradient produced by surface waves, which is represented in terms of the undisturbed free-stream velocity $U_\infty(t)$. The displacements of the seawater-mud and mud-seabed interfaces are $\eta(x,t)$ and $\zeta(x,t)$, respectively. The symbols are defined in the text and in the notation section.

$$\frac{\partial \eta}{\partial t}+\frac{\partial}{\partial x}[(h+\eta-\zeta)u]=0\,, \tag{2}$$

and an approximation to the layer-averaged momentum equation:

$$\frac{\partial u}{\partial t}+u\frac{\partial u}{\partial x}+g'\frac{\partial \eta}{\partial x}+\frac{\tau/\rho}{h+\eta-\zeta}=\frac{\rho_\infty}{\rho}\frac{dU_\infty}{dt}\,. \tag{3}$$

Here $\eta(x,t)$ is the displacement of the mud-water interface, $\zeta(x,t)$ is the displacement of the mud-seabed interface, $u(x, t)$ is the layer-averaged velocity within the fluid mud, $g'=g(\rho-\rho_\infty)/\rho$ is the reduced gravity, and $\tau(x,t)$ is the boundary shear stress at the seabed, modeled by

$$\frac{\tau}{\rho}=\frac{3\nu u}{h+\eta-\zeta}\,, \tag{4}$$

as in steady channel flow [e.g., *Batchelor*, 2000]. In (2) and (3), the evolution of the seabed has been assumed sufficiently slow that the seabed displacement ζ can be treated as time independent for the purpose of analyzing the wave-induced oscillatory flow within the fluid mud. The left side of (3) is a conventional layer-averaged approximation with a passive upper layer [e.g., *Pedlosky*, 1992], in which the horizontal velocity within the fluid mud has been approximated as vertically uniform, and vertical accelerations in both the upper and lower layers have been neglected. The right side of (3) represents the forcing by the undisturbed pressure gradient. The inertial terms that have been neglected in the upper and lower layers in (3) can be shown by scaling arguments to be of order kh and k^2h^2, respectively, in comparison with the leading terms, where k is the radian wave number of the interfacial waves and bed forms.

The evolution of the seabed is modeled by the mass-conservation equation for the sediment and the Meyer-Peter-Mueller parameterization of bed load sediment transport [e.g., *Fredsoe and Deigaard*, 1994], which can be combined to yield

$$(1-n)\frac{\partial \zeta}{\partial t}+\frac{\partial}{\partial x}\left[C\frac{\overline{|\tau|^{1/2}\tau}}{\rho^{3/2}g(s-1)}\right]=0\,, \tag{5}$$

where C is a dimensionless empirical constant, approximately equal to 8, and overbars denote expected values or time averages over several periods of the oscillatory forcing. In (5), the bed forms have been assumed to evolve over many periods of the oscillatory forcing, so that the second term on the left side, representing the divergence of the sediment flux within the seabed, is expressed in terms of the expected value. In addition, the seabed stresses have been assumed sufficiently large that the threshold effect of the critical stress required for the initiation of sediment motion can be neglected.

2.3. Undisturbed Flow

In the undisturbed case, the interfacial and seabed displacements $\eta(x,t)$ and $\zeta(x,t)$ are zero, and the layer-averaged velocity within the fluid mud, independent of x and denoted $U(t)$, is determined by setting $u(x,t)=U(t)$ and $\eta=\zeta=0$ in the momentum equation (3), resulting in

$$\frac{dU}{dt}+rU=\frac{\rho_\infty}{\rho}\frac{dU_\infty}{dt}\,, \tag{6}$$

where $r=3\nu/h^2$ is a damping rate. The solution to (6) is

$$U=\frac{\rho_\infty}{\rho}\frac{\omega^2 U_\infty+r\dot{U}_\infty}{\omega^2+r^2}\,. \tag{7}$$

Like U_∞, $U(t)$ is Gaussian and satisfies $d^2U/dt^2=-\omega^2U$.

2.4. Perturbed Flow

The linearized problem for the perturbed flow is obtained by subtracting the solution for the undisturbed flow from (2), (3), and (4), and retaining terms up to the lowest order in the small quantities η, ζ, and $u - U$. The resulting expressions can be combined to produce a single equation that determines the interfacial displacement η in terms of the seabed displacement ζ in the presence of the oscillatory forcing represented by U:

$$\left(\frac{\partial}{\partial t}+U\frac{\partial}{\partial x}\right)^2\eta+r\left(\frac{\partial}{\partial t}+3U\frac{\partial}{\partial x}\right)\eta-g'h\frac{\partial^2\eta}{\partial x^2}=\left(\frac{dU}{dt}+3rU\right)\frac{\partial\zeta}{\partial x}+U^2\frac{\partial^2\zeta}{\partial x^2}\,. \tag{8}$$

Here ζ has been treated, as noted above, as time independent for the purpose of analyzing the wave-induced flow within the fluid mud. The corresponding linear approximation to (5) is

$$\frac{\partial\zeta}{\partial t}=\frac{3}{2}\frac{C}{1-n}\frac{r^{3/2}h^{1/2}}{g(s-1)}\overline{|U|^{1/2}\left(\frac{\partial\eta}{\partial t}+2U\frac{\partial\eta}{\partial x}\right)}\,. \tag{9}$$

Here $\overline{|\tau|^{1/2}\tau}=\overline{|T|^{1/2}T}+(3/2)\overline{|T|^{1/2}\theta}+O(\theta^2)=(3/2)\overline{|T|^{1/2}\theta}+O(\theta^2)$ has been introduced, where $T=\rho rhU$ is the undisturbed stress, θ is the stress perturbation, and $|T|^{1/2}T\propto|U|^{1/2}U=0$ follows from the Gaussian statistics of U.

The linearized problem for the coupled evolution of the fluid mud and seabed is (8) and (9), with U given by (7). The mechanical properties of the seawater, fluid mud, and seabed are assumed known, as are the variance $\overline{U_\infty^2}$ and dominant radian frequency ω of the wave-induced forcing. The task is to solve for the interfacial and seabed displacements η and ζ. The procedure is first to solve (8), with ζ treated as time independent, to determine the relatively rapid fluctuations of the interfacial displacement η, and then to substitute the result into (9) to determine the slower evolution of the seabed displacement ζ.

3. Model Solutions

3.1. Unforced Case

In the unforced case ($U = 0$), (8) reduces to

$$\frac{\partial^2\eta}{\partial t^2}+r\frac{\partial\eta}{\partial t}-g'h\frac{\partial^2\eta}{\partial x^2}=0\,. \tag{10}$$

Spatially periodic solutions to (10) are

$$\eta(x,t)\propto\Re\left[e^{-rt/2+ikx\pm it\sqrt{g'hk^2-r^2/4}}\right], \tag{11}$$

where i is the imaginary unit. For $g'hk^2>r^2/4$, (11) represents two oscillatory modes, both damped at rate $r/2$, with radian frequencies $\pm\sqrt{g'hk^2-r^2/4}$. For $g'hk^2<r^2/4$, (11) represents two nonoscillatory modes, one strongly damped, and the other weakly damped at a rate that tends toward zero as $k\to0$. All modes described by (11) for nonzero r and k are damped, so that (10) and (11) do not describe the observed interfacial waves that were described in section 1.

3.2. Forced Case Without Bed Forms

In the forced case without bed forms ($U\neq0$ and $\zeta=0$), (8) reduces to

$$\left(\frac{\partial}{\partial t}+U\frac{\partial}{\partial x}\right)^2\eta+r\left(\frac{\partial}{\partial t}+3U\frac{\partial}{\partial x}\right)\eta-g'h\frac{\partial^2\eta}{\partial x^2}=0\,. \tag{12}$$

Spatially periodic solutions to (12) have the form

$$\eta(x,t)=\Re\left[A(t)e^{-rt/2+ikx-ik\int^t U(t')\,dt'}\right], \tag{13}$$

where t' is a dummy variable of integration and $A(t)$ is a complex amplitude that satisfies

$$\frac{d^2A}{dt^2}+\left(g'hk^2-\frac{r^2}{4}+2irkU\right)A=0, \tag{14}$$

which, with $U(t)\propto\cos(\omega t)$, is a dimensional form of the Mathieu equation [e.g., *Abramowitz and Stegun*, 1965] with an imaginary argument.

Solutions to (14) have the Floquet form $e^{\mu t}Q(t)$, where $Q(t)$ is periodic with the same period as $U(t)$. Instability occurs if the real part of the Floquet exponent μ, which can be calculated numerically by standard methods [e.g., *Abramowitz and Stegun*, 1965], is greater than the damping rate $r/2$ indicated by the exponential term in (13). The mechanism is a parametric viscous instability in which the term $2irkU$ in (14) resonates weakly damped modes described by (11). The mechanism is similar to the instability that causes surface waves in channel flow over a flat plat oscillating in its own plane [*Yih*, 1968; *Or*, 1997; *Gao and Lu*, 2006], and is related to other parametric instabilities in viscous oscillatory flows [e.g., *Yoshikawa and Wesfreid*, 2011a,b]. Instability in (14) requires that the squared Froude number $(\rho_\infty/\rho)^2\overline{U_\infty^2}/(g'h)$ exceed a threshold dependent on r/ω and the dimensionless wave number $k\sqrt{g'h}/\omega$, with favored growth near $k\sqrt{g'h}/\omega=1$, qualitatively consistent with the observations [*Traykovski et al.*, 2015], for $r/\omega=O(1)$.

The dependence on the wave number is weak, and the dominant dependence on the Froude number and r/ω can be obtained from an asymptotic solution for small wave number, following *Yih* [1968], *Or* [1997], and *Gao and Lu* [2006], which yields (Appendix A):

$$\mu-\frac{r}{2}=\frac{g'hk^2}{r}\left[\frac{4r^2\omega^2}{(r^2+\omega^2)^2}\left(\frac{\rho_\infty}{\rho}\right)^2\frac{\overline{U_\infty^2}}{g'h}-1\right]+O(k^4). \tag{15}$$

Instability requires that $\mu-r/2$ be positive, which requires in turn that the quantity in square brackets also be positive. The function of r/ω that multiplies the squared Froude number has a maximum value of unity at $r/\omega=1$ and vanishes for both small and large r/ω. The criterion for instability is not satisfied in the observations (Table 1 and Figure 1). Thus, although potentially important in other contexts, the parametric instability described by (12), (14), and (15) does not explain the interfacial waves that were described in section 1.

3.3. Forced Case With Bed Forms

In the forced case with bed forms ($U\neq 0$ and $\zeta\neq 0$), the solution procedure, as stated above in section 2.4, is first to solve (8), with ζ treated as time independent, to determine the relatively rapid fluctuations of the interfacial displacement η, and then to substitute the result into (9), to determine the slower evolution of the seabed displacement ζ. The analysis addresses disturbances that vary sinusoidally with x, so that $\partial^2\eta/\partial x^2=-k^2\eta$ and $\partial^2\zeta/\partial x^2=-k^2\zeta$. Although not capturing all of the phenomena described by (8) and (9), an approximate solution for small Keulegan-Carpenter number $\epsilon=O(kU/\omega)$, which is the ratio of the particle excursion U/ω to the bed form scale k^{-1}, describes the features of interest here. The method (Appendix B) is a standard perturbation procedure [e.g., *Bender and Orszag*, 1999]. The solution is carried to order ϵ^2, which is the lowest order at which a nonzero contribution to (9) occurs.

The solution to (8) for the interfacial displacement $\eta(x,t)$ with the bed form displacement ζ treated as time independent is

$$\eta=\left(\alpha_1\frac{U}{\omega}+\beta_1\frac{\dot U}{\omega^2}\right)\frac{\partial\zeta}{\partial x}+\left(\alpha_2\frac{U^2}{\omega^2}+\beta_2\frac{U\dot U}{\omega^3}+\gamma_2\frac{\overline{U^2}}{\omega^2}\right)\frac{\partial^2\zeta}{\partial x^2}+\ldots, \tag{16}$$

where α_1, β_1, α_2, β_2, and γ_2 are functions of $g'hk^2/\omega^2$ and r/ω (Appendix B). Note that (16) determines the interfacial displacement in response to not only slowly evolving bed forms, which are of primary interest here, but also fixed bed forms, which might be of interest in some applications.

The slow evolution of the bed forms is determined by substitution of (7) and (16) into (9), which yields, after computation of the required expected values,

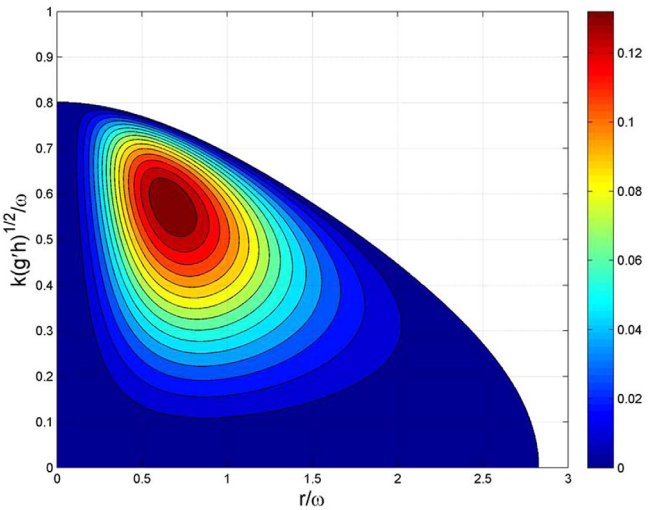

Figure 3. Dimensionless function G as a function of the frictional parameter $r/\omega = 3\nu/(\omega h^2)$ and the dimensionless wave number $k\sqrt{g'h}/\omega$. The color scale indicates the magnitude of G where G is positive. Negative values of G are indicated by white.

$$\frac{1}{\omega\zeta}\frac{\partial\zeta}{\partial t} = \frac{C}{(s-1)(1-n)}\left(\frac{\rho-\rho_\infty}{\rho}\right)\left(\frac{\omega^2 h}{g'}\right)^{3/4}\left(\frac{\rho_\infty^2}{\rho^2}\frac{\overline{U_\infty^2}}{g'h}\right)^{5/4} G\left(\frac{r}{\omega}, \frac{g'hk^2}{\omega^2}\right), \tag{17}$$

where G is a dimensionless function of its two arguments (Appendix B). Equation (17), together with the definition of G (Appendix B), gives the growth rate, nondimensionalized by the dominant radian frequency ω, for bed forms, and interfacial waves are described in turn by (16). The dimensionless growth rate $(\omega\zeta)^{-1}(\partial\zeta/\partial t)$ depends on the specific gravity s and the porosity n of the sediment, the dimensionless density contrast $(\rho-\rho_\infty)/\rho$, the dimensionless layer depth $\omega^2 h/g'$, the squared Froude number $(\rho_\infty^2/\rho^2)\overline{U_\infty^2}/(g'h)$, and, through the function G, the dimensionless damping rate $r/\omega = 3\nu/(\omega h^2)$ and the dimensionless wave number $k\sqrt{g'h}/\omega$. The function G is positive, indicating exponential growth, only for r/ω less than approximately 2.8 and $k\sqrt{g'h}/\omega$ less than approximately 0.80, and it is maximal for $r/\omega \simeq 0.67$ and $k\sqrt{g'h}/\omega \simeq 0.58$ (Figure 3).

The model solution is qualitatively consistent with the observations [*Traykovski et al.*, 2015] in indicating nearly instantaneous response of the interfacial waves to forcing by the surface wave groups (Figure 1), a dominant interfacial wave frequency equal to the dominant frequency of the surface waves (Figure 1), and bed form and interfacial wavelengths much shorter than the surface wavelength, but comparable to the wavelength given by the linear dispersion relationship for unforced interfacial waves, and much larger than lengths of wave-formed sand ripples in clear water under similar forcing (Table 1). Under strong forcing, the model time scales for bed form growth (Table 1) are sufficiently short that the bed forms can remain in approximate equilibrium with the variability of the surface wave statistics on the time scale of storms. In contrast, under weak forcing, the model time scales for growth are sufficiently long that the bed forms cannot keep up with variability in the statistics of the wave forcing, so that the bed forms likely reflect earlier conditions with stronger forcing, as in wave-formed ripples in clear water [e.g., *Traykovski*, 2007].

4. Discussion

4.1. Physics of the Forced Case With Bed Forms

In the model solution for the forced case with bed forms (section 3.3), the first term on the right side of (16) indicates standing interfacial waves with radian frequency ω, nodes over the bed form crests and troughs, and antinodes over the bed form slopes (Figure 4); and the second term on the right side indicates smaller standing interfacial waves with radian frequencies 2ω and zero, nodes over the bed form slopes, and antinodes over the bed form crests and troughs. Through the dependence of the seabed stress on U, $u - U$, and η in (4), these standing waves produce spatially varying seabed stresses at radian frequencies of zero, ω and

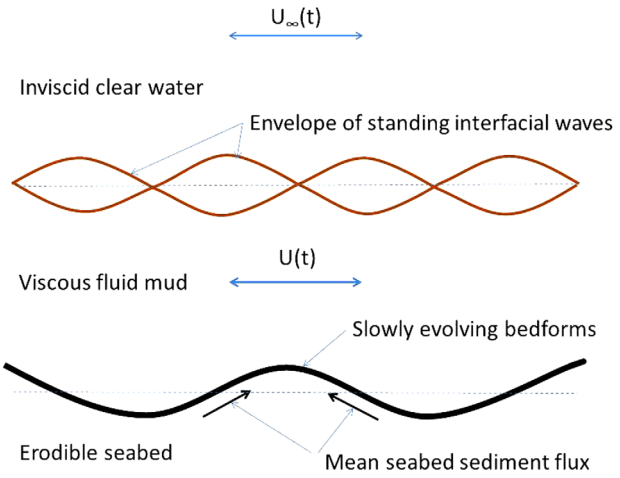

Figure 4. Diagram of the features indicated by the model solution for the forced case with bed forms. The slowly evolving bed forms in the presence of the rapid oscillatory flow excite standing waves on the interface between the fluid mud and the overlying clear seawater. At the lowest order in the Keulegan-Carpenter number, the interfacial waves have the same frequency as the surface waves and the same wavelength as the bed forms, with nodes over the bed form crests and troughs and antinodes over the bed form slopes, as shown here. At second order in the Keulegan-Carpenter number, the interfacial waves force a flow field that drives a wave-averaged or mean flux of sediment within the seabed, which, under favorable conditions, is toward the bed form crests, as shown here, thus causing bed form growth.

2ω, which interact with the undisturbed seabed stress to produce a time-averaged bed load sediment flux with a nonzero divergence (Figure 4), leading to bed form evolution as described by (17). Under favorable conditions, the divergence of the bed load sediment flux is negative over the bed form crests and positive over the bed form troughs, causing growth of the bed forms, which in turn amplifies the forcing of the interfacial waves, leading to exponential growth of both the bed forms and the interfacial waves. The most rapid growth occurs for r/ω of order unity and favors wave numbers of order $\omega/\sqrt{g'h}$ (Figure 3). The qualitative results do not depend strongly on the details of the model, i.e., the parameterization of the seabed stress or the sediment flux within the erodible seabed.

In the above mechanism, the two mechanical properties of the fluid mud, i.e., its density contrast and viscosity, play complementary roles. A nonzero density contrast permits interfacial waves, which can resonate and thus maximize the bed form growth rate at wave numbers approximately satisfying the linear long frictionless dispersion relationship (1). A nonzero viscosity damps the interfacial waves, thus slowing the response, but also creates the boundary shear stresses that produce the sediment transport within the erodible seabed that leads to bed form growth under favorable conditions. If the density contrast approaches zero ($\rho-\rho_\infty \to 0$), the bed form growth rate indicated by (17) approaches a finite value that is independent of the wave number and positive for order-one values of r/ω, indicating that the mud-seabed system remains unstable, but the growth rate is well below the maximum achieved for nonzero density contrasts, because the resonant response of the interfacial waves does not exist. If the viscosity approaches zero ($r/\omega \to 0$), the response of the interfacial waves to the oscillatory forcing imposed by the overlying flow in the presence of nonzero bed forms is, according to the solution (16), infinite at wave numbers satisfying (1), but the growth rate of the bed forms indicated by (17) is zero because there is no sediment transport in the underlying erodible seabed. If the viscosity approaches infinity ($r/\omega \to +\infty$), the flow within the mud layer vanishes because of strong friction, and the bed form growth is consequently zero. Thus, the mud-seabed system is most unstable at order-one values of $k\sqrt{g'h}/\omega$, near resonance of the interfacial waves, and order-one values of r/ω, with friction sufficiently weak to permit the near-resonant response of the interfacial waves, but strong enough to produce significant sediment fluxes and bed form growth within the erodible seabed.

4.2. Implications for Mixing and Control of Mud Layer Properties

Traykovski et al. [2015] suggested that the observed interfacial waves might be responsible for initiating mixing of the fluid mud with the overlying column of clear water, which presumably influences the thickness, density, and viscosity of the mud layer, and thus the impact of the fluid mud on the damping of surface waves. Mixing increases the layer thickness h and reduces the density ρ and the viscosity ν, thus decreasing the dimensionless frictional parameter $r/\omega=3\nu/(\omega h^2)$. In contrast, gravitational settling reduces h and increases ρ and ν, thus increasing r/ω. If the competing processes of mixing and settling occur with nearly the same mass of fluid mud always in suspension, then $g'h \propto (\rho-\rho_\infty)h$ does not change as the mud layer mixes or settles, and the dominant factor affecting stability of the mud-seabed system to bed forms, interfacial waves, and mixing is the dimensionless function G.

Qualitative inferences follow. Points such as A′ in Figure 5, to the left of the maximum in G as a function of r/ω, although unstable to interfacial waves, should be stable to changes in the layer thickness, density, and

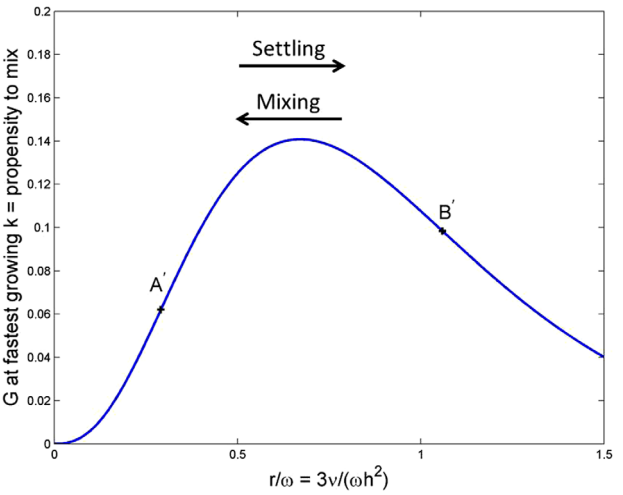

Figure 5. Diagram showing the competition between mixing and settling, as described in the text. The system remains on the blue curve, and mixing and settling drive the system to the left and right, respectively. At points such as A′, to the left of the maximum in the dimensionless growth rate *G*, the competition between mixing and settling should tend to maintain the thickness of the fluid mud layer at an approximately constant value. At points such as B′, to the right of the maximum in *G*, the fluid mud should tend to either mix or settle rapidly. Thus, fluid muds in nature should be observed only to the left of the maximum in *G* (at points such as A′), and never to the right of the maximum in *G* (at points such as B′), consistent with the observations.

viscosity. At these points, a small amount of settling moves the system toward greater r/ω, thus increasing *G*, creating mixing, and restoring the system toward the original value of r/ω. Conversely, a small amount of mixing decreases r/ω, thus decreasing *G*, suppressing mixing, and allowing settling, again restoring the system to the original value of r/ω. In contrast, at points such as B′ in Figure 5, to the right of the maximum in *G*, the system should be unstable to changes in the layer thickness and viscosity, in the sense that a small amount of mixing will create ever greater mixing, and a small amount of settling will produce ever greater settling. Thus, fluid muds in nature should be observed at points such as A′ and never at points such as B′.

It is noteworthy that all three of the cases identified by *Traykovski et al*. [2015] correspond to points such as A′ (Table 1), to the left of the maximum in *G* (Figure 5), and the two cases with the shortest time scales for bed form growth, when the bed forms and interfacial waves are most nearly in equilibrium with the instantaneous forcing, are near the point where $dG/d(r/\omega)$ is maximal (Figure 3), which should be where the system is at its most resistant to changing configuration through the competition between mixing and settling.

5. Summary and Conclusions

Motivated by observations indicating interfacial waves and bed forms in fluid muds over erodible seabeds in the presence of ocean surface waves, a linear model has been formulated for oscillatory forcing of viscous fluid mud overlain by clear inviscid seawater and in turn overlying an erodible seabed. The model is based on the layer-averaged mass equation and the hydrostatic momentum equation for the mud layer, modeled as an incompressible Newtonian fluid, and the Meyer-Peter-Mueller model of bed load sediment transport within the underlying erodible seabed. In the unforced case, the model solutions are temporally damped spatially periodic interfacial disturbances. In the forced case without bed forms, the model indicates a parametric instability in which the periodic variability of the viscous stress resonates interfacial disturbances, similar to the previously studied parametric resonance of surface waves in channel flow over a flat plate oscillating in its own plane; however, the threshold for instability indicated by the model is not met in the observations. In the forced case with bed forms, an approximate solution for small Keulegan-Carpenter number indicates an instability in which bed forms force interfacial waves, which in turn create stresses in the fluid mud that under favorable conditions transport sediment toward the bed form crests, thus causing growth of both bed forms and interfacial waves. This mechanism requires that the viscous parameter $r/\omega{=}3\nu/(\omega h^2)$ and the dimensionless wave number $k\sqrt{g'h}/\omega$ be within order-one ranges. The model computations of preferred wavelengths and growth rates of interfacial waves and bed forms are qualitatively consistent with the observations. The qualitative results do not depend strongly on the details of the model. Model results suggest that a competition between gravitational settling and vertical mixing produced by the unstable interfacial waves might maintain the fluid mud during active forcing at values of $r/\omega{=}3\nu/(\omega h^2)$ that are less than approximately unity, in qualitative agreement with the observations, thus impacting the properties of the fluid muds and their effects on the damping of ocean surface waves.

Appendix A: Asymptotic Solution for Parametric Resonance Over a Flat Seabed

Substitution of the Floquet form $A(t)=Q(t)e^{\mu t}$ into (14) yields

$$\ddot{Q}+2\mu\dot{Q}+\left(\mu^2+g'hk^2-\frac{r^2}{4}+2irkU\right)Q=0\,. \tag{A1}$$

Following *Yih* [1968], *Or* [1997], and *Gao and Lu* [2006], assume for small k

$$Q(t)=Q_0(t)+kQ_1(t)+k^2Q_2(t)+\ldots \text{ and } \mu=\mu_0+k\mu_1+k^2\mu_2+\ldots\,. \tag{A2}$$

Substitution of (A2) into (A1) yields a sequence of problems ordered by k. At zeroth order,

$$\ddot{Q}_0+2\mu_0\dot{Q}_0+\left(\mu_0^2-\frac{r^2}{4}\right)Q_0=0\,. \tag{A3}$$

The solution with periodic Q_0 and positive μ_0 is

$$Q_0=\text{constant and } \mu_0=\frac{r}{2}\,. \tag{A4}$$

At first order,

$$\ddot{Q}_1+r\dot{Q}_1+(r\mu_1+2irU)Q_0=0\,. \tag{A5}$$

The solution with periodic Q_1 is

$$Q_1=\frac{2ir}{r^2+\omega^2}\left(U+\frac{r}{\omega^2}\dot{U}\right)Q_0 \text{ and } \mu_1=0\,. \tag{A6}$$

At second order,

$$\ddot{Q}_2+r\dot{Q}_2+2irUQ_1+(r\mu_2+g'h)Q_0=0\,. \tag{A7}$$

With periodic Q_2, the time average of (A7) over many periods of the oscillatory forcing gives

$$\mu_2=-\frac{2i}{Q_0}\overline{UQ_1}-\frac{g'h}{r}\,. \tag{A8}$$

Use of (A4), substitution of (A6) and (7) into (A8), and recollection of (A2) yield (15).

Appendix B: Solution for Coupled Growth of Bed Forms and Interfacial Waves

Let $U=\epsilon U_1$, where $U_1=O(\omega/k)$, and assume that

$$\eta(x,t)=\epsilon\eta_1(x,t)+\epsilon^2\eta_2(x,t)+\ldots. \tag{B1}$$

Substitution of (B1) into (8) yields a sequence of problems ordered by ϵ. The first-order problem is

$$\frac{\partial^2\eta_1}{\partial t^2}+r\frac{\partial\eta_1}{\partial t}+g'hk^2\eta_1=\left(\frac{dU_1}{dt}+3rU_1\right)\frac{\partial\zeta}{\partial x}\,. \tag{B2}$$

The first-order solution is

$$\eta_1=\left(\alpha_1\frac{U_1}{\omega}+\beta_1\frac{\dot{U}_1}{\omega^2}\right)\frac{\partial\zeta}{\partial x}\,, \tag{B3}$$

where

$$\alpha_1=\frac{(r/\omega)(3g'hk^2/\omega^2-2)}{(g'hk^2/\omega^2-1)^2+r^2/\omega^2} \text{ and } \beta_1=\frac{g'hk^2/\omega^2-1-3r^2/\omega^2}{(g'hk^2/\omega^2-1)^2+r^2/\omega^2}\,. \tag{B4}$$

The second-order problem is

$$\frac{\partial^2\eta_2}{\partial t^2}+r\frac{\partial\eta_2}{\partial t}+g'hk^2\eta_2=-\frac{dU_1}{dt}\frac{\partial\eta_1}{\partial x}-2U_1\frac{\partial^2\eta_1}{\partial x\partial t}-3rU_1\frac{\partial\eta_1}{\partial x}+U_1^2\frac{\partial^2\zeta}{\partial x^2}\,, \tag{B5}$$

or, after substitution of (B3),

$$\frac{\partial^2\eta_2}{\partial t^2}+r\frac{\partial\eta_2}{\partial t}+g'hk^2\eta_2=\left[-3\left(\alpha_1+\frac{r}{\omega}\beta_1\right)\frac{U_1\dot{U}_1}{\omega}+\left(1-3\frac{r}{\omega}\alpha_1+3\beta_1\right)U_1^2-2\beta_1\overline{U_1^2}\right]\frac{\partial^2\zeta}{\partial x^2}\,. \tag{B6}$$

The second-order solution is

$$\eta_2=\left(\alpha_2\frac{U_1^2}{\omega^2}+\beta_2\frac{U_1\dot{U}}{\omega^3}+\gamma_2\frac{\overline{U_1^2}}{\omega^2}\right)\frac{\partial^2\zeta}{\partial x^2}\,, \tag{B7}$$

where α_2, β_2, and γ_2 are functions of r/ω and $g'hk^2/\omega^2$. Of these quantities, the present analysis requires only

$$\beta_2=\frac{3(4-g'hk^2/\omega^2)[\alpha_1+(r/\omega)\beta_1]-2(r/\omega)[1-3(r/\omega)\alpha_1+3\beta_1]}{(g'hk^2/\omega^2-4)^2+4(r/\omega)^2}\,. \tag{B8}$$

By substituting (B3) and (B7) into (B1) and recalling the definitions of ϵ and U_1, one obtains (16). By substituting (B1), (B3), and (B7) into (9), and introducing the expected values

$$\overline{|U|^{1/2}}=\frac{2^{1/4}}{\sqrt{\pi}}\Gamma\left(\frac{3}{4}\right)\left(\overline{U^2}\right)^{1/4}\ \text{and}\ \overline{|U|^{1/2}U^2}=\frac{3}{2}\overline{|U|^{1/2}}\cdot\overline{U^2}\,, \tag{B9}$$

one obtains (17), where

$$G=\frac{3\Gamma(3/4)}{2^{3/4}\sqrt{\pi}}\frac{(r/\omega)^{3/2}(\beta_2-3\alpha_1)}{(1+r^2/\omega^2)^{5/4}}\frac{g'hk^2}{\omega^2}\,, \tag{B10}$$

in which Γ is the gamma function [e.g., *Abramowitz and Stegun*, 1965].

Notation

$A(t)$	complex amplitude in the solution for the forced case without bed forms.
C	dimensionless constant in the Meyer-Peter Mueller equation for bed load sediment transport.
g	magnitude of the gravitational acceleration.
g'	reduced gravitational acceleration $= g(\rho-\rho_\infty)/\rho$.
G	function of r/ω and $g'hk^2/\omega^2$ in the solution for the forced case with bed forms.
h	constant undisturbed thickness of the fluid mud layer.
i	imaginary unit $=\sqrt{-1}$.
k	real wave number of the interfacial disturbances and bed forms.
$P(x,z,t)$	undisturbed pressure in the fluid mud.
r	damping rate $3\nu/(\omega h^2)$.
t	time.
t'	dummy variable of integration.
$T(t)$	undisturbed shear stress at the mud-seabed interface.
$U(t)$	undisturbed horizontal layer-averaged velocity in the fluid mud.
$U_\infty(t)$	undisturbed horizontal velocity in the overlying clear seawater.
x	horizontal coordinate.
ϵ	small parameter of order kU/ω in the solution for the forced case with bed forms.
$\eta(x,t)$	displacement of the interface between the fluid mud and the overlying clear water.
$\theta(x,t)$	perturbed shear stress at the mud-seabed interface.
ν	constant kinematic viscosity of the fluid mud.
ρ	constant density of the fluid mud.
ρ_∞	constant density of the overlying clear seawater.
ω	dominant radian frequency of the forcing by the surface waves
$\tau(x,t)$	boundary shear stress at the seabed.
$\bar{\phi}$	expected value (or time average over many wave periods) of an arbitrary quantity $\phi(t)$.
$\dot{\phi}$	time derivative $\partial\phi/\partial t$ of an arbitrary function $\phi(t)$.

Acknowledgments
This study was supported by the Coastal Geodynamics Program at the Office of Naval Research and by the Physical Oceanography Program at the National Science Foundation. The authors are grateful to Gail Kineke for useful discussions. Data used in this study are available in *Traykovski et al.* [2015]. For further details about the data or higher resolution, please contact Peter Traykovski at ptraykovski@whoi.edu.

References

Abramowitz, M., and I. A. Stegun (1965), *Handbook of Mathematical Functions*, Natl. Bur. of Stand., Washington, D. C.
Batchelor, G. K. (2000), *An Introduction to Fluid Dynamics*, Cambridge Univ. Press, N. Y.
Bender, C. M., and S. A. Orszag (1999), *Advanced Mathematical Methods for Scientists and Engineers*, Springer, N. Y.
Dalrymple, R. A., and P. L. F. Liu (1978), Waves over soft muds: A two-layer fluid model, *J. Phys. Oceanogr.*, *8*, 1121–1131.
Drazin, P. G., and W. H. Reid (2004), *Hydrodynamic Stability*, Cambridge Univ. Press, N. Y.
Fredsoe, J., and R. Deigaard (1994), *Mechanics of Coastal Sediment Transport*, World Sci., Singapore.
Gade, H. (1958), Effects of a non-rigid, impermeable bottom on plane surface waves in shallow water, *J. Mar. Res.*, *16*, 61–82.
Gao, P., and X. Y. Lu (2006), Effect of surfactants on the long-wave stability of oscillatory film flow, *J. Fluid Mech.*, *562*, 345–354.
Harang, A., O. Thual, P. Brancher, and T. Bonometti (2014), Kelvin-Helmholtz instability in the presence of variable viscosity for mudflow resuspension in estuaries, *Environ. Fluid Mech.*, *14*, 743–769, doi:10.1007/s10652-014-9337-4.
Hill, D. F., and M. A. Foda (1996), Subharmonic resonance of short internal standing waves by progressive surface waves, *J. Fluid Mech.*, *321*, 217–233.
Hill, D. F., and M. A. Foda (1998), Subharmonic resonance of oblique interfacial waves by a progressive surface wave, *Proc. R. Soc. London, Ser. A*, *454*, 1129–1144.
Hill, D. F., and M. A. Foda (1999), Effects of viscosity and elasticity on the nonlinear resonance of internal waves, *J. Geophys. Res.*, *104*(C5), 10,951–10,957.
Hsiao, S., and O. Shemdin (1980), Interaction of ocean waves with a soft bottom, *J. Phys. Oceanogr.*, *10*, 605–610.
Jamali, M., B. Seymour, and G. A. Lawrence (2003a), Asymptotic solution of a surface-interfacial wave interaction, *Phys. Fluids*, *15*, 47–55.
Jamali, M., G. A. Lawrence, and B. Seymour (2003b), A note on the resonant interaction between a surface wave and two interfacial waves, *J. Fluid Mech.*, *491*, 1–9.
Jiang, F., and A. Mehta (1995), Mudbanks of the southwest coast of India IV: Mud viscoelastic properties, *J. Coastal. Res.*, *11*, 918–926.
Jiang, F., and A. Mehta (1996), Mudbanks of the southwest coast of India V: Wave attenuation, *J. Coastal Res.*, *12*, 890–897.
Kaihatu, J., and J. Kirby (1995), Nonlinear transformation of waves in finite water depth, *Phys. Fluids*, *7*, 1903–1914.
Kaihatu, J., A. Sheremet, and T. Holland (2007), A model for the propagation of nonlinear surface waves over viscous muds, *Coastal Eng.*, *54*, 752–764.
Liu, K., and C. C. Mei (1989), Effects of wave-induced friction on a muddy seabed modeled as a Bingham-plastic fluid, *J. Coastal Res.*, *SI5*, 777–789.
MacPherson, H. (1980), The attenuation of water waves over a non-rigid bed, *J. Fluid Mech.*, *97*, 721–742.
Ng, C. (2000), Water waves over a muddy bed: A two layer Stokes boundary layer model, *Coastal Eng.*, *40*, 221–242.
Or, A. C. (1997), Finite-wavelength instability in a horizontal liquid layer on an oscillating plane, *J. Fluid Mech.*, *335*, 213–232.
Pedlosky, J. (1992), *Geophysical Fluid Dynamics*, Springer, N. Y.
Traykovski, P. (2007), Observations of wave orbital scale ripples and a nonequilibrium time-dependent model, *J. Geophys. Res.*, *112*, C06026, doi:10.1029/2006JC003811.
Traykovski, P., J. H. Trowbridge, and G. Kineke (2015), Mechanisms of surface wave energy dissipation over a high concentration sediment suspension, *J. Geophys. Res. Oceans*, *120*, 1638–1681, doi:10.1002/2014JC010245.
Wiberg, P. L., and C. K. Harris (1994), Ripple geometry in wave-dominated environments, *J. Geophys. Res.*, *99*(C1), 775–789.
Wintertwerp, J., R. de Graaff, J. Groeneweg, and A. Luijendijk (2007), Modelling of wave damping at Guyana mud coast, *Coastal Eng.*, *54*, 249–261.
Yih, C. S. (1968), Instability of unsteady flows or configurations, part I, instability of a horizontal liquid layer on an oscillating plane, *J. Fluid Mech.*, *38*, 273–278.
Yoshikawa, H., and J. E. Wesfreid (2011a), Oscillatory Kelvin-Helmholtz instability. Part 1. A viscous theory, *J. Fluid Mech.*, *675*, 223–248.
Yoshikawa, H., and J. E. Wesfreid (2011b), Oscillatory Kelvin-Helmholtz instability. Part 2. An experiment in fluids with a large viscosity contrast, *J. Fluid Mech.*, *675*, 249–267.